

# Measurement of Muon Neutrino Quasi-Elastic Scattering on Carbon

A. A. Aguilar-Arevalo<sup>5</sup>, A. O. Bazarko<sup>12</sup>, S. J. Brice<sup>7</sup>, B. C. Brown<sup>7</sup>, L. Bugel<sup>5</sup>, J. Cao<sup>11</sup>, L. Coney<sup>5</sup>, J. M. Conrad<sup>5</sup>, D. C. Cox<sup>8</sup>, A. Curioni<sup>16</sup>, Z. Djurcic<sup>5</sup>, D. A. Finley<sup>7</sup>, B. T. Fleming<sup>16</sup>, R. Ford<sup>7</sup>, F. G. Garcia<sup>7</sup>, G. T. Garvey<sup>9</sup>, C. Green<sup>7,9</sup>, J. A. Green<sup>8,9</sup>, T. L. Hart<sup>4</sup>, E. Hawker<sup>15</sup>, R. Imlay<sup>10</sup>, R. A. Johnson<sup>3</sup>, P. Kasper<sup>7</sup>, T. Katori<sup>8</sup>, T. Kobilarcik<sup>7</sup>, I. Kourbanis<sup>7</sup>, S. Koutsoliotas<sup>2</sup>, E. M. Laird<sup>12</sup>, J. M. Link<sup>14</sup>, Y. Liu<sup>11</sup>, Y. Liu<sup>1</sup>, W. C. Louis<sup>9</sup>, K. B. M. Mahn<sup>5</sup>, W. Marsh<sup>7</sup>, P. S. Martin<sup>7</sup>, G. McGregor<sup>9</sup>, W. Metcalf<sup>10</sup>, P. D. Meyers<sup>12</sup>, F. Mills<sup>7</sup>, G. B. Mills<sup>9</sup>, J. Monroe<sup>5</sup>, C. D. Moore<sup>7</sup>, R. H. Nelson<sup>4</sup>, P. Nienaber<sup>13</sup>, S. Ouedraogo<sup>10</sup>, R. B. Patterson<sup>12</sup>, D. Perevalov<sup>1</sup>, C. C. Polly<sup>8</sup>, E. Prebys<sup>7</sup>, J. L. Raaf<sup>3</sup>, H. Ray<sup>9</sup>, B. P. Roe<sup>11</sup>, A. D. Russell<sup>7</sup>, V. Sandberg<sup>9</sup>, R. Schirato<sup>9</sup>, D. Schmitz<sup>5</sup>, M. H. Shaevitz<sup>5</sup>, F. C. Shoemaker<sup>12</sup>, D. Smith<sup>6</sup>, M. Sorel<sup>5</sup>, P. Spentzouris<sup>7</sup>, I. Stancu<sup>1</sup>, R. J. Stefanski<sup>7</sup>, M. Sung<sup>10</sup>, H. A. Tanaka<sup>12</sup>, R. Tayloe<sup>8</sup>, M. Tzanov<sup>4</sup>, R. Van de Water<sup>9</sup>, M. O. Wascko<sup>10</sup>, D. H. White<sup>9</sup>, M. J. Wilking<sup>4</sup>, H. J. Yang<sup>11</sup>, G. P. Zeller<sup>5</sup>, E. D. Zimmerman<sup>4</sup>

(The MiniBooNE Collaboration)

<sup>1</sup>University of Alabama; Tuscaloosa, AL 35487

<sup>2</sup>Bucknell University; Lewisburg, PA 17837

<sup>3</sup>University of Cincinnati; Cincinnati, OH 45221

<sup>4</sup>University of Colorado; Boulder, CO 80309

<sup>5</sup>Columbia University; New York, NY 10027

<sup>6</sup>Embry-Riddle Aeronautical University; Prescott, AZ 86301

<sup>7</sup>Fermi National Accelerator Laboratory; Batavia, IL 60510

<sup>8</sup>Indiana University; Bloomington, IN 47405

<sup>9</sup>Los Alamos National Laboratory; Los Alamos, NM 87545

<sup>10</sup>Louisiana State University; Baton Rouge, LA 70803

<sup>11</sup>University of Michigan; Ann Arbor, MI 48109

<sup>12</sup>Princeton University; Princeton, NJ 08544

<sup>13</sup>Saint Mary's University of Minnesota; Winona, MN 55987

<sup>14</sup>Virginia Polytechnic Institute & State University; Blacksburg, VA 24061

<sup>15</sup>Western Illinois University; Macomb, IL 61455

<sup>16</sup>Yale University; New Haven, CT 06520

(Dated: June 7, 2007)

Low energy ( $200 < E_\nu < 2000$  MeV) neutrino oscillation experiments, including MiniBooNE, require a model of charged current quasi-elastic (CCQE) neutrino interactions to predict signal samples. Using a high-statistics sample of muon neutrino CCQE events, MiniBooNE finds that a simple Fermi gas model, with appropriate adjustments, accurately characterizes the CCQE events observed in a carbon-based detector. The extracted parameters include an effective axial mass,  $M_A = 1.23 \pm 0.20$  GeV, used to describe the four-momentum dependence of the axial-vector form factor of the nucleon; and a Pauli-suppression parameter,  $\kappa = 1.019 \pm 0.011$ .

Charged current quasi-elastic (CCQE,  $\nu_\mu n \rightarrow \mu^- p$ ) events dominate neutrino interactions at energies between 200 – 2000 MeV. Because the process has a large cross section and identifies both the incident neutrino flavor and energy, it forms an ideal signal sample in neutrino oscillation experiments. To ensure high event yields, typical experiments use nuclear media such as carbon, water, or iron for their neutrino targets. As a result, a detailed understanding of quasi-elastic scattering on nuclear targets is required. To model the scattering from nucleons confined in nuclei, most neutrino oscillation experiments employ an event generator based on the relativistic Fermi gas (RFG) model [1]. Such models assume a flat nucleon momentum distribution up to some Fermi momentum ( $p_F$ ), assign a nuclear binding energy ( $E_B$ ) to account for nuclear interactions in the initial and final states, and utilize standard nucleon vector and axial-

vector on-shell form factors. Many of these model parameters may be inferred from existing data; for example,  $p_F$ ,  $E_B$ , and the vector form factors can be determined from elastic electron scattering data [2, 3]. Despite providing these constraints, electron data yield limited information on the axial-vector form factor of the nucleon and the CCQE cross section at very low four-momentum transfer ( $Q^2$ ). Present knowledge of the axial-vector form factor has been informed largely by past neutrino experiments, but these suffer from low statistics and were performed using predominantly deuterium targets [4]. Since these early measurements, neutrino experiments have encountered difficulties describing their data at low  $Q^2$ , where nuclear effects are largest, and have often measured axial-vector form factor parameters above some minimum  $Q^2$  value.

The MiniBooNE experiment has collected the largest

sample of low energy muon neutrino CCQE events to date. We describe here the use of such events in tuning the RFG model to better describe quasi-elastic scattering on nuclear targets. The analysis fits the reconstructed  $Q^2$  distribution of the MiniBooNE CCQE data in the region  $0 < Q^2 < 1 \text{ GeV}^2$  to a simple RFG model [1] with two adjustable parameters: the axial mass,  $M_A$ , appearing in the axial-vector form factor; and  $\kappa$ , a parameter that adjusts the level of Pauli-blocking at low values of  $Q^2$ . The best-fit model results in a good description of the data across the full kinematic phase space including the low- $Q^2$  region. This technique is crucial to the MiniBooNE oscillation search [5] because it allows the prediction of  $\nu_e$  CCQE oscillation events based on the constraints provided by the high-statistics MiniBooNE  $\nu_\mu$  CCQE sample.

The Fermilab Booster neutrino beam, optimized for the MiniBooNE oscillation search, is particularly suited for investigation of low energy neutrino interactions. The Fermilab Booster provides 8.89 GeV/c protons which collide with a 71 cm long beryllium target inside a magnetic horn. The horn focuses positively charged pions and kaons produced in these collisions, which can subsequently decay in a 50 m long decay region, yielding an intense flux of muon neutrinos. A geant4-based [6] beam simulation uses a parametrization [7] of pion production cross sections based on recent measurements from the HARP [8] and E910 [9] experiments, along with a detailed model of the beamline geometry to predict the neutrino flux as a function of neutrino energy and flavor. The resulting flux of neutrinos at the MiniBooNE detector is predicted to be 93.8% (5.7%)  $\nu_\mu$  ( $\bar{\nu}_\mu$ ) with a mean energy of  $\sim 700 \text{ MeV}$ . Because 99% of the flux lies below 2.5 GeV, the background from high multiplicity neutrino interactions is small. Approximately 40% of the total events at MiniBooNE are predicted to be  $\nu_\mu$  CCQE, of which 96% result from pion decays in the beam.

The MiniBooNE detector is a spherical tank of inner radius 610 cm filled with 800 tons of mineral oil ( $\text{CH}_2$ ), situated 541 meters downstream of the proton target. An optical barrier divides the detector into two regions, an inner volume with a radius of 575 cm and an outer volume 35 cm thick. The inner region of the tank houses 1280 inward-facing 8 inch photomultiplier tubes (PMTs), providing 10% photocathode coverage. The outer region is lined with 240 pair-mounted PMTs which provide a veto for charged particles entering or leaving the tank. Muons produced in CCQE interactions emit primarily Cherenkov light with a small amount of scintillation light. The majority of muons stop and decay in the main detector volume. The muon kinetic energy resolution is 7% at 300 MeV and the angular resolution is  $5^\circ$ . The response of the detector to muons is calibrated using a dedicated muon tagging system that independently measures the muon energy for cosmic ray muons ranging up

to 800 MeV.

Neutrino interactions within the detector are simulated with the v3 nuance event generator [10]. This program provides the framework for tuning the CCQE cross section parameters (described below) and predicts backgrounds to the sample, including neutrino induced single pion production events ( $\text{CC } 1\pi$ ). Pion interactions in the nucleus and photon emission from nuclear de-excitation in nuance are tuned to reproduce MiniBooNE and other [11] data. A geant3-based [12] detector model (with gcalor [13] hadronic interactions) simulates the detector response to particles produced in neutrino interactions. The simulation of light production and propagation in mineral oil has been tuned using external small-sample measurements [14], muon decay electrons (also used to calibrate the energy scale), and recoil nucleons from neutrino neutral current (NC) elastic scattering events. The predicted events are additionally overlaid with events measured in a beam-off gate, in order to incorporate backgrounds from natural radioactivity and cosmic rays into the simulated data.

Because of the low energy neutrino beam and MiniBooNE detector capabilities, the identification of  $\nu_\mu$  CCQE interactions relies solely on the detection of the primary muon and associated decay electron in these events:

$$\nu_\mu + n \rightarrow \mu^- + p, \quad \mu^- \rightarrow e^- + \nu_\mu + \bar{\nu}_e.$$

This simple selection is highly effective for several reasons. First, the efficiency for detecting the decay of the  $\mu^-$  produced in such events is high, with only an 8% inefficiency due to the  $\mu^-$  capture probability on carbon [15]. Second, the  $\text{CC } 1\pi^+$  contamination is significantly reduced by requiring a single decay electron, since  $\text{CC } 1\pi^+$  events typically yield two decay electrons, one each from the primary muon and the  $\pi^+$  decay chains. The exceptions are cases in which the primary  $\mu^-$  is captured or, more likely, the  $\pi^+$  is either absorbed or undergoes a charge-changing interaction in the target nucleus or detector medium. Each of these processes is included in the detector simulation. Finally, by avoiding requirements on the outgoing proton kinematics, the selection is inherently less dependent on nuclear models.

Timing information from the PMTs allows the light produced by the initial neutrino interaction (first “sub-event”) to be separated from light produced by the decay electron (second sub-event). The time and charge response of the PMTs is used to reconstruct the position, kinetic energy, and direction vector of the primary particle within each sub-event. Once separated into sub-events, we require that the first sub-event (the neutrino interaction) must occur in coincidence with a beam pulse, have a reconstructed position  $< 500 \text{ cm}$  from the center of the detector, possess  $< 6$  veto-PMT hits to ensure containment, and have  $> 200$  main-PMT hits to avoid electrons from cosmic ray muon decays. The second sub-

event (the  $\mu^-$  decay electron) must have  $< 6$  veto-PMT hits and  $< 200$  main-PMT hits. Subsequent cuts specifically select  $\nu_\mu$  CCQE events and discriminate against CC  $1\pi^+$  backgrounds. First, events must contain exactly two sub-events. Second, the distance between the electron vertex and muon track endpoint must be less than 100 cm, ensuring that the decay electron is associated with the muon track.

A total of 193,709 events pass the MiniBooNE  $\nu_\mu$  CCQE selection criteria from  $5.58 \times 10^{20}$  protons on target collected between August 2002 and December 2005. The cuts are estimated to be 35% efficient at selecting  $\nu_\mu$  CCQE events in a 500 cm radius, with a CCQE purity of 74%.

The predicted backgrounds are: 74.8% CC  $1\pi^+$ , 15.0% CC  $1\pi^0$ , 4.0% NC  $1\pi^\pm$ , 2.6% CC multi- $\pi$ , 0.9% NC elastic, 0.8%  $\bar{\nu}_\mu$  CC  $1\pi^-$ , 0.8% NC  $1\pi^0$ , 0.6%  $\eta/\rho/K$  production, and 0.5% deep inelastic scattering and other events. Because pions can be absorbed via final state interactions in the target nucleus, a large fraction of the background events look like CCQE events in the MiniBooNE detector. “CCQE-like” events, all events with a muon and no pions in the final state, are predicted to be 84% of the sample after cuts.

The observables in the MiniBooNE  $\nu_\mu$  CCQE sample are the muon kinetic energy  $T_\mu$ , and the muon angle with respect to the neutrino beam direction  $\theta_\mu$ . The high-statistics MiniBooNE data sample allows us to verify the simulation in two dimensions. Figure 1 shows the level of agreement between the shape of the data and simulation in the CCQE kinematic quantities before any CCQE cross section model adjustments. For this comparison, the simulation assumes the RFG model as implemented in nuance [1, 10], with  $E_B = 34$  MeV [2],  $p_F = 220$  MeV/c [2], and updated non-dipole vector form factors [3]. The axial-vector form factor is assumed to have a dipole form as a function of  $Q^2$  with one adjustable parameter,  $M_A$ , the so-called “axial mass”:

$$F_A(Q^2) = g_A / (1 + Q^2/M_A^2)^2. \quad (1)$$

The simulation shown in Fig. 1 specifically assumes  $g_A = 1.2671$  [16] and  $M_A = 1.03$  GeV [17]. These model parameters are common defaults in most neutrino simulations. The figure shows that the disagreement between data and simulation follows lines of constant  $Q^2$  and not  $E_\nu$ . This supports the assumption that the data/model disagreement is not due to a mis-modeling of the incoming neutrino energy spectrum but an inaccuracy in the simulation of the CCQE process itself.

Guided by indications that the data-model discrepancy is only a function of  $Q^2$ , we have modified the existing  $\nu_\mu$  CCQE model rather than introduce more drastic changes to the cross section calculation. This approach works well and requires adjustment of only two parameters:  $M_A$  and  $E_{lo}$ . The parameter  $E_{lo}$  effectively controls the strength of Pauli-blocking. It is the lower bound of integration

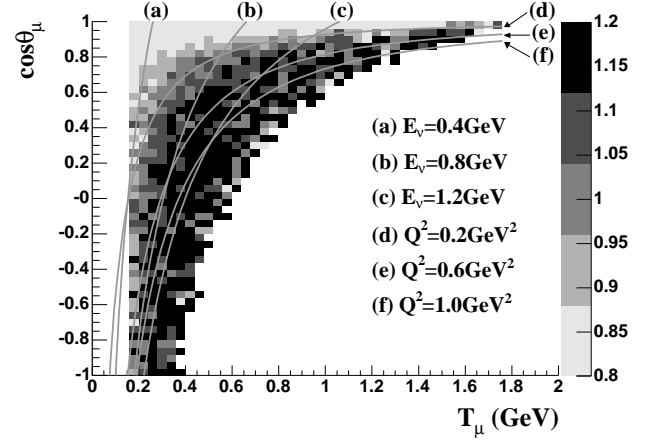


FIG. 1: Ratio of MiniBooNE  $\nu_\mu$  CCQE data/simulation as a function of reconstructed muon angle and kinetic energy. The prediction is prior to any CCQE model adjustments; the  $\chi^2/\text{dof} = 79.5/53$ . The ratio forms a 2D surface whose values are represented by the gray scale, shown on the right. If the simulation modelled the data perfectly, the ratio would be unity everywhere. Contours of constant  $E_\nu$  and  $Q^2$  are overlaid, and only bins with  $> 20$  events in the data are plotted.

over initial state nucleon energy and appears within the RFG model together with an upper bound  $E_{hi}$ :

$$E_{hi} = \sqrt{p_F^2 + M_n^2}, \quad E_{lo} = \sqrt{p_F^2 + M_p^2} - \omega + E_B, \quad (2)$$

where  $M_n$  is the target neutron mass,  $M_p$  is the outgoing proton mass, and  $\omega$  is the energy transfer. In the RFG model,  $E_{hi}$  is the energy of an initial nucleon on the Fermi surface and  $E_{lo}$  is the lowest energy of an initial nucleon that leads to a final nucleon just above the Fermi momentum (and thus obeying the exclusion principle in the final state). In practice, a simple scaling of  $E_{lo}$  was implemented in the MiniBooNE CCQE data fit via  $E_{lo} = \kappa(\sqrt{p_F^2 + M_p^2} - \omega + E_B)$ . The parameter  $\kappa$  adds a degree of freedom to the RFG model which can describe the smaller cross section observed in the data at low momentum transfer. Adjustment of both parameters,  $M_A$  and  $\kappa$ , is likely compensating for an inadequate nucleon momentum distribution in the RFG model.

The adjusted RFG model is then fit to the shape of the reconstructed  $Q^2$  distribution in the MiniBooNE  $\nu_\mu$  CCQE data:

$$Q^2 = -q^2 = -m_\mu^2 + 2E_\nu(E_\mu - p_\mu \cos \theta_\mu) > 0, \quad (3)$$

where  $m_\mu$  is the muon mass,  $E_\mu$  ( $p_\mu$ ) is the reconstructed muon energy (momentum), and  $\theta_\mu$  is the reconstructed muon scattering angle. The reconstructed neutrino energy  $E_\nu$  is formed assuming the target nucleon is at rest inside the nucleus:

$$E_\nu = \frac{2(M_n - E_B)E_\mu - (E_B^2 - 2M_n E_B + m_\mu^2 + \Delta M^2)}{2[(M_n - E_B) - E_\mu + p_\mu \cos \theta_\mu]}, \quad (4)$$

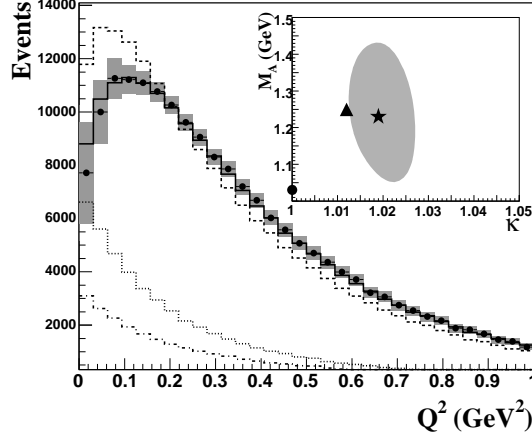


FIG. 2: Reconstructed  $Q^2$  for  $\nu_\mu$  CCQE events including systematic errors. The simulation, before (dashed) and after (solid) the fit, is normalized to data. The dotted (dot-dash) curve shows backgrounds that are not CCQE (not “CCQE-like”). The inset shows the  $1\sigma$  CL contour for the best-fit parameters (star), along with the starting values (circle), and fit results after varying the background shape (triangle).

where  $\Delta M^2 = M_n^2 - M_p^2$  and  $E_B > 0$ . A small correction is applied to  $E_\nu$  in both data and simulation to account for the biasing effects of Fermi-smearing. This procedure, while yielding a more accurate  $E_\nu$  estimate, has a negligible impact on the  $Q^2$  fit to MiniBooNE CCQE data. These expressions, with reconstructed muon kinematics, yield an  $E_\nu$  resolution of 11% and a  $Q^2$  resolution of 21% for CCQE events.

The model parameters  $M_A$  and  $\kappa$  are obtained from a least-squares fit to the measured data in 32 bins of reconstructed  $Q^2$  from 0 to 1  $\text{GeV}^2$ . All other parameters of the model are held fixed to the values listed previously, and a complete set of correlations between systematic uncertainties is considered. The total prediction is normalized to the data for each set of parameter values. Thus, the procedure is sensitive only to the shape of the  $Q^2$  distribution, and any changes in the total cross section due to parameter variation do not impact the quality of fit. The  $Q^2$  distributions of data and simulation before and after the fitting procedure are shown in Figure 2. The  $\chi^2/\text{dof}$  of the fit is 32.8/30 and the parameters extracted from the MiniBooNE  $\nu_\mu$  CCQE data are:

$$M_A = 1.23 \pm 0.20 \text{ GeV}; \quad (5)$$

$$\kappa = 1.019 \pm 0.011. \quad (6)$$

While normalization is not explicitly used in the fit, the new model parameters increase the predicted rate of  $\nu_\mu$  CCQE events at MiniBooNE by 5.6%.

In general, varying  $M_A$  allows us to reproduce the high  $Q^2$  behavior of the observed data events. A fit for  $M_A$  above  $Q^2 > 0.25 \text{ GeV}^2$  yields consistent results,  $M_A =$

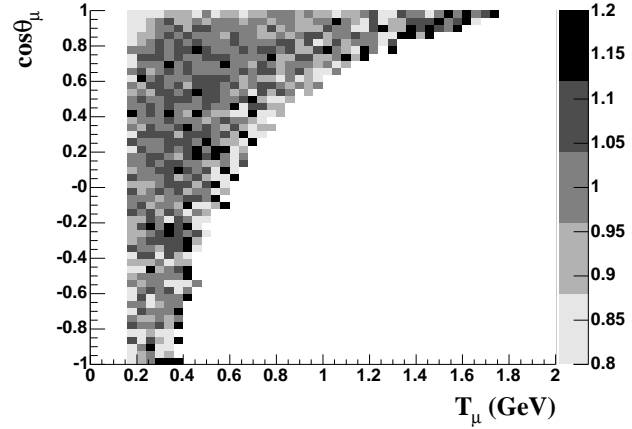


FIG. 3: Ratio of data/simulation as a function of muon kinetic energy and angle after CCQE model adjustments; the  $\chi^2/\text{dof} = 45.1/53$ . Compare to Figure 1.

TABLE I: Uncertainties in  $M_A$  and  $\kappa$  from the fit to MiniBooNE  $\nu_\mu$  CCQE data. The total error is not a simple quadrature. sum because of the correlation between the two parameters.

error source	$\delta M_A$	$\delta \kappa$
data statistics	0.03	0.003
neutrino flux	0.04	0.003
neutrino cross sections	0.06	0.004
detector model	0.10	0.003
CC $\pi^+$ background shape	0.02	0.007
total error	0.20	0.011

$1.25 \pm 0.12 \text{ GeV}$ . However, fits varying only  $M_A$  across the entire  $Q^2$  range leave considerable disagreement at low  $Q^2$  ( $\chi^2/\text{dof} = 48.8/31$ ). The Pauli-blocking parameter  $\kappa$  is instrumental here, enabling this model to match the behavior of the data down to  $Q^2 = 0$  (Figure 2).

Figure 3 shows the agreement between data and simulation after incorporation of the  $M_A$  and  $\kappa$  values from the  $Q^2$  fit to MiniBooNE data. Comparing to Figure 1, the improvement is substantial and the data are well-described throughout the kinematic phase space.

Table I shows the contributions to the systematic uncertainties on  $M_A$  and  $\kappa$ . The detector model uncertainties dominate the error in  $M_A$  due to their impact on the energy and angular reconstruction of CCQE events in the MiniBooNE detector. The dominant error on  $\kappa$  is the uncertainty in the  $Q^2$  shape of background events. This error (not included in the contour of Figure 2) is evaluated in a separate fit, where MiniBooNE CC  $1\pi^+$  data are used to set the background instead of the event generator prediction, and then added in quadrature.

The result reported here,  $M_A = 1.23 \pm 0.20 \text{ GeV}$ , is consistent with a recent K2K measurement on a water target,  $M_A = 1.20 \pm 0.12 \text{ GeV}$  [18]. Both val-



ues are systematically higher than the historical value,  $M_A = 1.026 \pm 0.021$  GeV, set largely by deuterium-based bubble chamber experiments [17]. The  $M_A$  value reported here should be considered an “effective parameter” in the sense that it may be incorporating nuclear effects not otherwise included in the RFG model. Future efforts will explore how the value of  $M_A$  extracted from the MiniBooNE data is altered upon replacement of the RFG model with more advanced nuclear models [19].

In summary, modern quasi-elastic scattering data on nuclear targets are revealing the inadequacies of present neutrino cross section simulations. Taking advantage of the high-statistics MiniBooNE  $\nu_\mu$  CCQE data, we have extracted values of an effective axial mass parameter,  $M_A = 1.23 \pm 0.20$  GeV, and a Pauli-blocking parameter,  $\kappa = 1.019 \pm 0.011$ , achieving substantially improved agreement with the observed kinematic distributions in this data set. Incorporation of both fit parameters allows, for the first time, a description of neutrino CCQE scattering on a nuclear target down to  $Q^2 = 0$  GeV<sup>2</sup>.

We wish to acknowledge the support of Fermilab, the Department of Energy, and the National Science Foundation in the construction, operation, and data analysis of the MiniBooNE experiment.

---

[1] R.A. Smith and E.J. Moniz, Nucl. Phys. **B43**, 605 (1972);  
*erratum: ibid.* **B101**, 547 (1975).

[2] E.J. Moniz *et al.*, Phys. Rev. Lett. **26**, 445 (1971); the binding energy is 25 MeV from electron scattering data plus 9 MeV from the  $T = 0, 1$  splitting plus Coulomb corrections.

[3] R. Bradford *et al.*, Nucl. Proc. Suppl. **159**, 127 (2006).

[4] S.K. Singh and E. Oset, Nucl. Phys. **A542**, 587 (1992).

[5] A. A. Aguilar-Arevalo *et al.*, hep-ex/0704.1500v2.

[6] S. Agostinelli *et al.*, Nucl. Instrum. Meth. **A506**, 250 (2003).

[7] J.R. Sanford and C.L. Wang, BNL AGS internal reports 11299 and 11479 (1967), unpublished.

[8] M.G. Catanesi *et al.*, hep-ex/0702024.

[9] I. Chemakin *et al.*, in preparation.

[10] D. Casper, Nucl. Phys. Proc. Suppl. **112**, 161 (2002).

[11] D. Ashery *et al.*, Phys. Rev. **C23**, 2173 (1981); H. Ejiri, Phys. Rev. **C48**, 1442 (1993); F. Ajzenberg-Selove, Nucl. Phys. **A506**, 1 (1990).

[12] CERN Program Library Long Writeup W5013 (1993).

[13] C. Zeitnitz and T.A. Gabriel, Nucl. Instrum. Meth. **A349**, 106 (1994).

[14] B.C. Brown *et al.*, IEEE Nuclear Science Symposium Conference Record 1, 652 (2004).

[15] T. Suzuki *et al.*, Phys. Rev. **C35**, 2212 (1987).

[16] W.M. Yao *et al.*, J. Phys. **G33**, 1 (2006).

[17] V. Bernard *et al.*, J. Phys. **G28**, R1 (2002).

[18] R. Gran *et al.*, Phys. Rev. **D74**, 052002 (2006).

[19] J.E. Amaro *et al.*, Phys. Rev. **C71**, 015501 (2005); T. Leitner *et al.*, Phys. Rev. **C73**, 065502 (2006); O. Benhar *et al.*, Phys. Rev. **D72**, 053005 (2005); S. Ahmad *et al.*, Phys. Rev. **D74**, 073008 (2006).